THE FASEB JOURNAL • RESEARCH • www.fasebj.org

Wnt3a involved in the mechanical loading on improvement of bone remodeling and angiogenesis in a postmenopausal osteoporosis mouse model

Xinle Li,[*,‡] Daquan Liu,[*,‡] Jie Li,[*] Shuang Yang,[*] Jinfeng Xu,[*] Hiroki Yokota,[†] and Ping Zhang[*,†,‡,1]

[*]Department of Anatomy and Histology, School of Basic Medical Sciences and [‡]Key Laboratory of Hormones and Development (Ministry of Health), Tianjin Key Laboratory of Metabolic Diseases, Tianjin Medical University, Tianjin, China; and [†]Department of Biomedical Engineering, Indiana University–Purdue University Indianapolis, Indiana, USA

ABSTRACT: Osteoporosis is a major health problem, making bones fragile and susceptible to fracture. Previous works showed that mechanical loading stimulated bone formation and accelerated fracture healing. Focusing on the role of Wnt3a (wingless/integrated 3a), this study was aimed to assess effects of mechanical loading to the spine, using ovariectomized (OVX) mice as a model of osteoporosis. Two-week daily application of this novel loading (4 N, 10 Hz, 5 min/d) altered bone remodeling with an increase in Wnt3a. Spinal loading promoted osteoblast differentiation, endothelial progenitor cell migration, and tube formation and inhibited osteoclast formation, migration, and adhesion. A transient silencing of Wnt3a altered the observed loading effects. Spinal loading significantly increased bone mineral density, bone mineral content, and bone area per tissue area. The loaded OVX group showed a significant increase in the number of osteoblasts and reduction in osteoclast surface/bone surface. Though expression of osteoblastic genes was increased, the levels of osteoclastic genes were decreased by loading. Spinal loading elevated a microvascular volume as well as VEGF expression. Collectively, this study supports the notion that Wnt3a-mediated signaling involves in the effect of spinal loading on stimulating bone formation, inhibiting bone resorption, and promoting angiogenesis in OVX mice. It also suggests that Wnt3a might be a potential therapeutic target for osteoporosis treatment.—Li, X., Liu, D., Li, J., Yang, S., Xu, J., Yokota, H., Zhang, P. Wnt3a involved in the mechanical loading on improvement of bone remodeling and angiogenesis in a postmenopausal osteoporosis mouse model. FASEB J. 33, 000–000 (2019). www.fasebj.org

KEY WORDS: OVX · neovascularization · bone resorption · bone formation · spinal load

Osteoporosis is a common skeletal disease, affecting 1 in 3 women during the course of their lifetime (1). It is characterized by reduced bone mass, microarchitectural deterioration of bone tissue, and an increased risk of fractures (2). Bone remodeling is a continuous process of mineral metabolism, undertaken mainly by bone-forming osteoblast cells and bone-resorbing osteoclast cells (3). Diminished bone formation by osteoblasts or excessive bone resorption by osteoclasts results in osteoporosis (4). In postmenopausal women, osteoporosis is induced by a decrease in the production of estrogen, which is known to maintain the appropriate ratio of osteoblasts to osteoclasts (5, 6). To treat postmenopausal osteoporosis, the most widely prescribed medications are bisphosphonates such as alendronate and zolendronic acid, although their long-term administration may increase the incidence of osteonecrosis of the jawbone and fracture of the femur (7, 8). Other treatments include administration of estrogen and estrogen analogs as well as parathyroid hormone (teriparatide) (9). However, increased risks of breast cancer and blood clots have been reported as side effects (10). Angiogenesis is essential for bone remodeling in the repair of the bone disorders such as fracture, osteonecrosis, and tumor metastasis to bone (11, 12). However, a therapy of osteoporosis coupling angiogenesis to bone remodeling

ABBREVIATIONS: ALP, alkaline phosphatase; B.Ar/T.Ar, bone area per tissue area; BMC, bone mineral content; BMD, bone mineral density; CTSK, cathepsin K; DAB, 3, 3′-diaminobenzidine; DMEM, Dulbecco's Modified Eagle's Medium; EGM-2, endothelial cell growth medium-2; EPC, endothelial progenitor cell; FBS, fetal bovine serum; H&E, hematoxylin and eosin; DMEM, Dulbecco's Modified Eagle's Medium; MEM-α, minimum essential medium alpha; NFATc1, nuclear factor of activated T cells cytoplasmic 1; N.Ob/BS, osteoblast number/bone surface; Oc.S/BS, osteoclast surface/bone surface; OCN, osteocalcin; OVX, ovariectomized; pDEXA, peripheral dual-energy X-ray absorptiometry; RANKL, receptor activator of nuclear factor κ-B ligand; RUNX2, runt-related transcription factor 2; siRNA, small interfering RNA; TRAP, tartrate-resistant acid phosphatase; VEGF, vascular endothelial growth factor; VEGFR2, vascular endothelial growth factor receptor 2; Wnt, wingless/integrated

[1] Correspondence: Department of Anatomy and Histology, School of Basic Medical Sciences, Tianjin Medical University, 22 Qixiangtai Rd., Tianjin 300070, China. E-mail: pizhang2008@163.com

doi: 10.1096/fj.201802711R

remains elusive. The aim of this study is to evaluate a potential therapeutic role of spinal loading as a physical therapy in postmenopausal osteoporosis, focusing on bone remodeling and angiogenesis.

Bone is a dynamic tissue whose structure is constantly altered in response to its mechanical environments (13). Indeed, many loading modalities including axial loading and whole-body vibration can influence the bone-remodeling process (14–16). Joint loading modalities have been developed and reported in our works (17), in which lateral loads are applied to synovial joints such as the elbow (18), knee (19–21), and ankle (22). Our previous studies showed that wound healing was stimulated with knee loading both in the femoral neck and tibia (23). Knee loading not only stimulates bone formation and prevents cartilage degeneration, but it also promotes vessel remodeling and bone healing in the necrotic femoral head (20, 24, 25). Spinal loading is one form of mechanical stimulation modalities, in which gentle compressive loads are dynamically applied to the lumbar spine. The question herein is whether spinal loading may induce not only local but also global anabolic responses in osteoporotic bones.

Mechanical loading activates a Wnt signaling pathway (25–27), and it plays a critical role in bone homeostasis (28). It stimulates osteoblastogenesis and bone formation through β-catenin–dependent or –independent mechanisms (29). Wnt signaling is also important for osteoclast differentiation and bone resorption (30). Furthermore, Wnt signaling is implicated in angiogenesis and the activation of VEGF expression (31).

We hypothesized that Wnt3a involves in the effect of spinal loading on promoting both bone remodeling and angiogenesis in ovariectomized (OVX) mice. Using bone marrow–derived cells, we examined formation, migration, and adhesion of osteoclasts as well as differentiation of osteoblasts. Endothelial progenitor cells (EPCs) from bone marrow were evaluated by their tube formation using Matrigel and a migration assay. To investigate a Wnt3a-mediated underlying mechanism, expression of varying genes involved in bone remodeling and angiogenesis were determined in bone marrow–derived cells using small interfering RNA (siRNA) specific to Wnt3a. Using the sham-treated OVX and OVX mice, we evaluated the effects of spinal loading on bone remodeling by determining bone mineral density (BMD), bone mineral content (BMC), and bone area per tissue area (B.Ar/T.Ar). Using bone histomorphometry, we evaluated development of osteoblasts and osteoclasts on bone surface *in vivo*. The vessels in the distal femora were evaluated with ink perfusion angiography.

MATERIALS AND METHODS

Animal and material preparation

Female C57BL/6 mice (14 wk old; Animal Center of Academy of Military Medical Sciences, Beijing, China) were used. A total of 150 mice were randomly divided into the following 3 groups: sham-treated control group (sham, $n = 50$), OVX group (OVX, $n = 50$), and spinal loading–treated OVX group (OVX loading, $n = 50$). Four to five mice per cage were fed with mouse chow and water *ad libitum*. Mice were housed on a 12-h light/dark cycle at room temperature of 25°C under pathogen-free conditions. All experiments were carried out according to the *Guide for the Care and Use of Laboratory Animals* (National Institutes of Health, Bethesda, MD, USA) and were approved by the Ethics Committee of Tianjin Medical University.

Cytokines were purchased from PeproTech (Rocky Hills, NC, USA). Medium, fetal bovine serum (FBS), bovine serum albumin, Lipofectamine 3000 Reagent, penicillin, streptomycin, and trypsin were purchased from Thermo Fisher Scientific (Waltham, MA, USA). Endothelial cell growth medium-2 (EGM-2) BulletKit was obtained from Lonza (Walkersville, MD, USA). Matrigel was purchased from Life Sciences (Tewksbury, MA, USA). Scrambled siRNA and Wnt3a siRNA were purchased from GenePharma (Shanghai, China). 3, 3′-diaminobenzidine (DAB) substrate kit was purchased from ZSGB-BIO (Beijing, China). Primary antibodies specific to Wnt3a, runt-related transcription factor 2 (RUNX2), osteocalcin (OCN), receptor activator of nuclear factor κ-B ligand (RANKL), and cathepsin K (CTSK) were purchased from Cell Signaling Technology (Danvers, MA, USA). The antibodies for alkaline phosphatase (ALP), nuclear factor of activated T cells, cytoplasmic 1 (NFATc1), vascular endothelial growth factor (VEGF), and β-actin were purchased from Abcam (Cambridge, MA, USA). Other chemicals were purchased from MilliporeSigma (Burlington, MA, USA) unless otherwise stated.

Ovariectomy

The animals were anesthetized with 1.5% isoflurane (IsoFlo; Abbott Laboratories, North Chicago, IL, USA) at a flow rate of 1.0 L/min. We placed the mouse in prone position, shaved the hair, and sterilized the skin. We made a midline dorsal skin incision using a scalpel and excised the ovaries with scissors (32). For sham-treated OVX-operated mice, the same procedure was conducted without removing the ovaries. In order to alleviate the pain associated with surgery, the mouse was administered a dose of 0.05 mg/kg buprenorphine hydrochloride every 8 h for the first 3 postoperative days. After surgery, 1% pramoxine hydrochloride ointment was applied on the incision sites everyday for the first 3 postoperative days.

In vivo mechanical stimulation

The OVX-loaded mice were subject to mechanical stimulation. During mechanical spinal loading, the mouse was mask-anesthetized using 1.5% isoflurane. A custom-made mechanical loader was employed to apply loads for 5 min/d for 2 wk (7 d/wk) to the lumbar spine in the dorsal-ventral direction (**Fig. 1*A***). The upper diameter of the loader was 10 mm, and it connected to a stator that is right above lumbar spine of mice (12 × 5 mm). A soft pad (60 × 15 mm) was placed on the loading table to support the mouse abdomen during spinal loading. Dynamic loads were given sinusoidally by the upper end of the stator moving up and down gently in proper force, frequency, and time. The OVX and sham-treated OVX groups received sham loading, in which mice were positioned on the loading table without receiving dynamic loading to the spine. After loading, the mouse was allowed normal cage activity. In the current study, loads with 10 Hz and 4 N were given for 5 min/d for 14 consecutive days. The loading force of 4 N was determined *via* preliminary experiment using 3 loading forces (2, 4, and 6 N; unpublished results). Though data indicated that all loading forces inhibited osteoclast

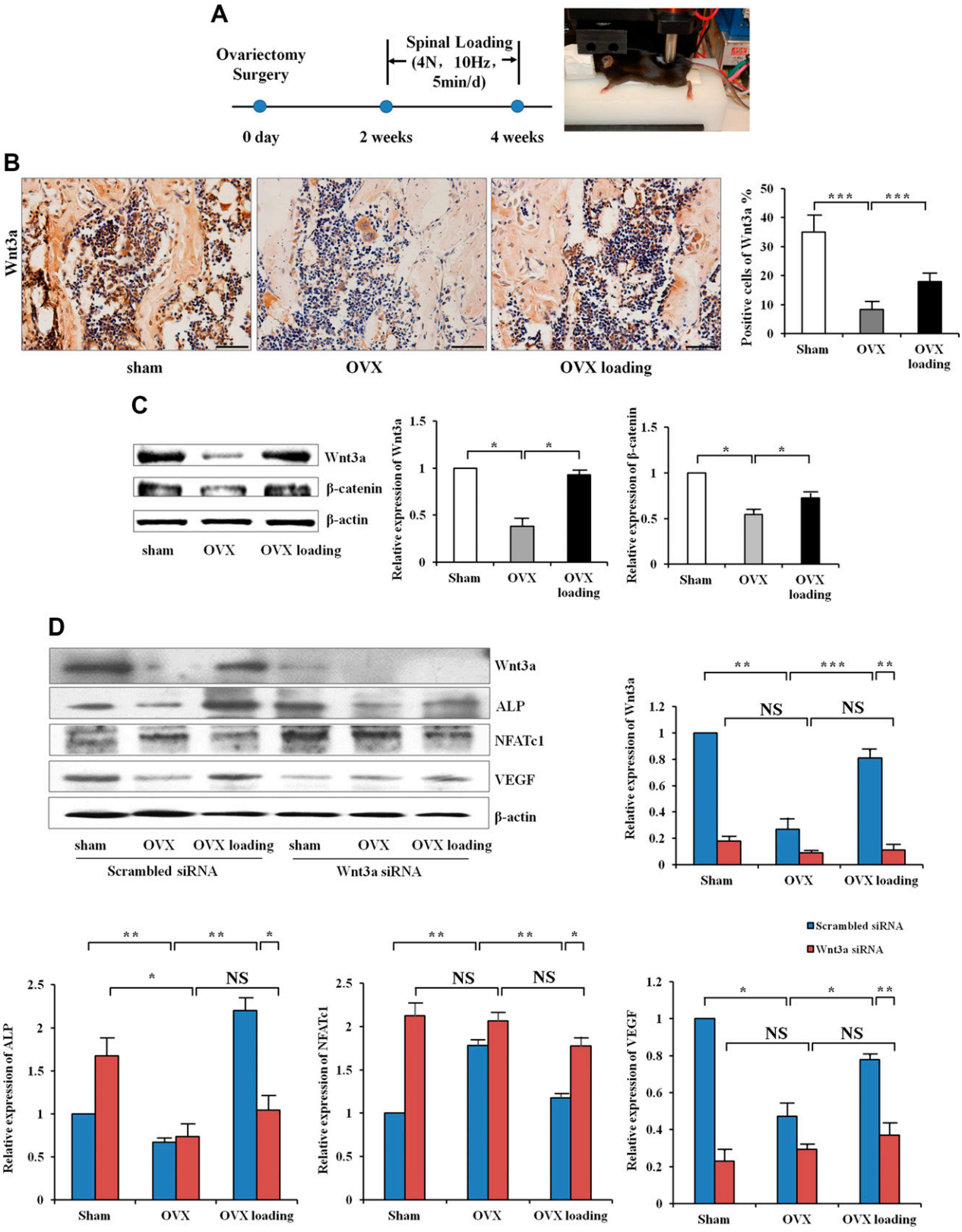

Figure 1. Role of Wnt3a in the effect of spinal loading on bone remodeling and angiogenesis in the OVX mice. *A*) Experimental setup. Timeline and loading site for spinal loading. *B*) Immunohistochemistry staining of Wnt3a in the femur was conducted *in vivo*. Scale bars, 50 μm; $n = 10$. *C*) Western blot analysis of Wnt3a and β-catenin in the femur of OVX treated with mechanical loading *in vivo* ($n = 6$). *D*) Western blot analysis of Wnt3a, ALP, NFATc1, and VEGF in bone marrow–derived cells, which were transfected with siRNA Wnt3a *in vitro* ($n = 6$). NS, not significant. $^*P < 0.05$, $^{**}P < 0.01$, $^{***}P < 0.001$.

development, forces of 4 and 6 N and not 2 N stimulated osteoblast differentiation. The loading device was calibrated using a load cell (Model LLB130; Futek Advanced Sensor Technology, Irvine, CA, USA) to determine peak compressive force for increasing actuator voltage.

Western blot analysis

Femurs were lysed in a RIPA lysis buffer to isolate proteins. Primary antibodies specific to Wnt3a, RUNX2, OCN, ALP, NFATc1, RANKL, CTSK, VEGF, and β-actin were employed. Signals were detected with ECL. Quantification of signal intensities was performed using the software Quantity One (Bio-Rad, Hercules, CA, USA), following the manufacturer's instructions. Signal intensities of Wnt3a, RUNX2, OCN, ALP, NFATc1, RANKL, CTSK, and VEGF were normalized to β-actin intensity (33).

Bone histomorphometry and immunohistochemistry

The femurs were fixed in 10% neutral buffered formalin for 2 d, decalcified in 10% EDTA (pH 7.4) for 2 wk, and embedded in paraffin. The samples were cut at 5-μm–thick slices along the coronal plane. Sections were stained with hematoxylin and eosin (H&E) for examining histologic parameters in the distal metaphysis. Bone volume fraction, B.Ar/T.Ar (in percent), was determined within 1.6-mm^2 sample area on 0.8 mm proximal distance from the growth plate (30). Furthermore, we used tartrate-resistant acid phosphatase (TRAP) staining to determine osteoclast surface/bone surface (Oc.S/BS; ratio of a length of TRAP-positive cells to a total circumference of bone trabecula), which represented osteoclast-activity. MacNeal's staining was used to normalize the osteoblast number by the trabecular bone surface (osteoblast number/bone surface, N.Ob/BS; mm) for identifying osteoblasts (24).

For immunohistochemistry, we used an immunohistochemical kit and a DAB substrate kit (ZSGB-BIO). The femurs were embedded in paraffin and coronally cut for 5-μm–thick slices. One of every 10 slices and a total of 5 slices were chosen for quantification in each tissue. Sections of the distal femur were incubated with primary antibodies against Wnt3a. Quantitative analysis was conducted in a blinded fashion on the area of the proximal femur. To quantify Wnt3a expression, we counted the number of positively stained cells in 10 fields at ×200 magnification per section and calculated the ratio of positively stained cells to all cells (34).

Transfection

Wnt3a siRNA was transfected into bone marrow–derived cells using Lipofectamine 3000 Reagent in antibiotic-free Opti-MEM following the manufacturer's protocol (35). Cells were incubated

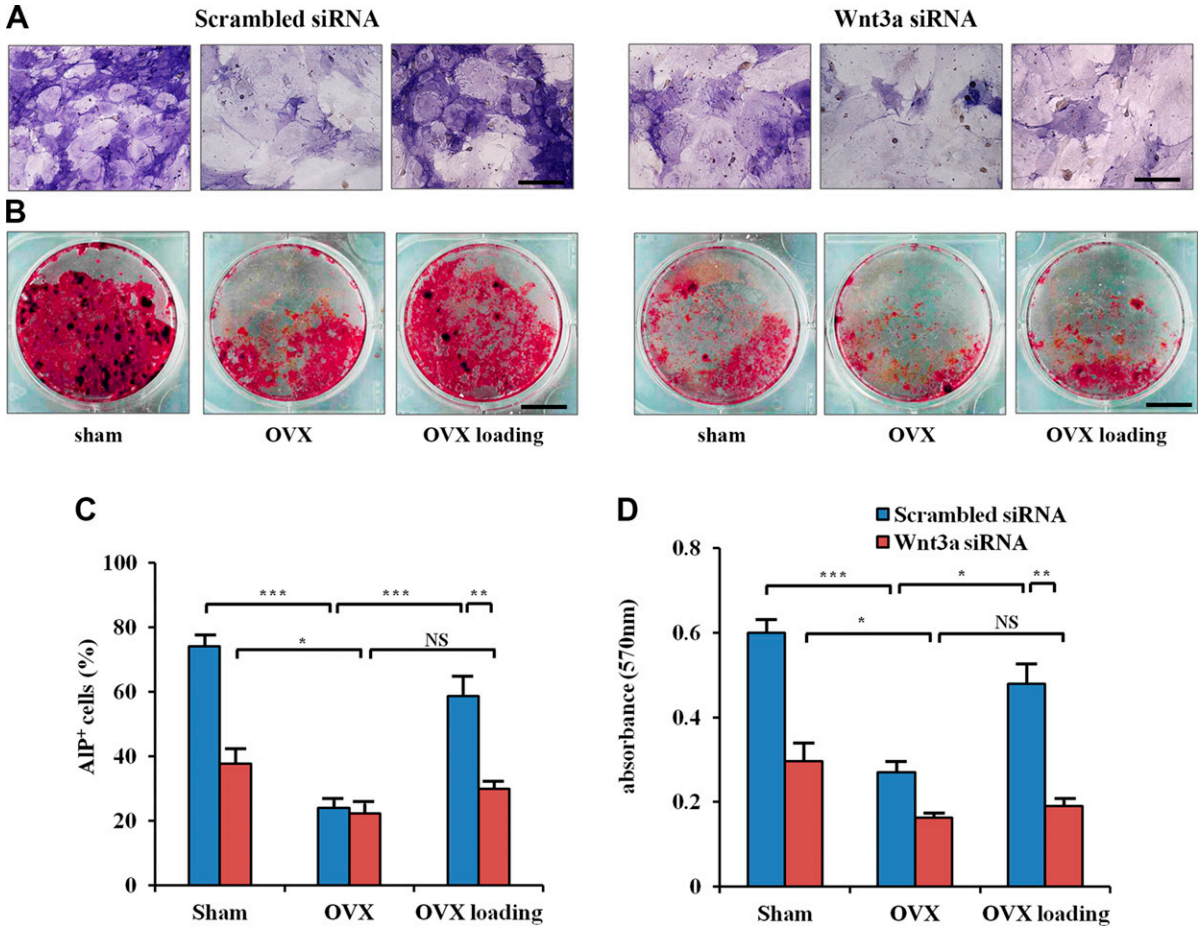

Figure 2. Effect of silencing Wnt3a on osteoblast differentiation and mineralization with spinal loading in OVX mice *in vitro*. *A*) Representative images of osteoblast differentiation by ALP staining. Scale bar, 50 μm. *B*) Representative images of osteoblast mineralization by Alizarin Red staining. Scale bar, 500 μm. *C*) Quantitative analysis of ALP$^+$ cells (percent). *D*) Optical density of calcium deposition after Alizarin Red staining. NS, not significant. $n = 6$ per treatment group. $^*P < 0.05$, $^{**}P < 0.01$, $^{***}P < 0.001$.

for 6 h, and the medium was replaced with Opti-MEM medium. Cells were incubated for 48 h after transfection and used for experiments.

Bone marrow–derived cell isolation and osteoclast development

Bone marrow–derived cells were collected as previously described in ref. 25. We flushed the iliac and femur with Dulbecco's Modified Eagle's Medium (DMEM) containing 2% FBS. Bone marrow–derived cells were separated by Ficoll density gradient centrifugation and seeded in 6-well dishes (36). Cells were cultured in minimum essential medium alpha (MEM-α) with 30 ng/ml murine macrophage-colony stimulating factor (M-CSF) and 20 ng/ml RANKL. On d 4, the medium of cells was replaced by MEM-α with 30 ng/ml M-CSF and 60 ng/ml RANKL and grown for 3 additional days (37, 38).

An osteoclast formation assay was performed using bone marrow–derived cells, which were isolated from the sham-treated OVX mice, OVX mice, and spine-loaded OVX mice, as previously described in refs. 34 and 37. During 6-d experiments, culture medium was exchanged once on d 4. Cells were fixed and stained with a TRAP-staining kit according to the manufacturer's instructions. TRAP-positive multinuclear cells (>3 nuclei) were identified as osteoclasts and their numbers were counted (39).

A transwell assay was conducted to evaluate migration of osteoclasts (34, 38). To obtain osteoclast precursor cells, bone marrow–derived cells (2×10^6/ml in 6-well plates) were cultured for 4 d, and TRAP staining was conducted to identify osteoclast precursors. The identified osteoclast precursor cells (1×10^5 cells/well) were loaded onto the upper chamber of transwells. The bottom chamber contained MEM-α with 1% bovine serum albumin and 30 ng/ml M-CSF. The cells in the lower chamber were stained with crystal violet and counted after 6 h.

The identified osteoclast precursor cells (1×10^5 cells/well) were placed into 96-well plates coated with 5 μg/ml vitronectin and 30 ng/ml M-CSF for an osteoclast adhesion assay, as previously described (34, 40). Cells were fixed with 4% paraformaldehyde for 10–15 min and stained with crystal violet. The number of adhesion cells was counted.

Osteoblast differentiation and mineralization assay

Bone marrow–derived cells (2×10^6/ml in 6-well plates) were plated to osteogenic differentiation medium with 10 mM

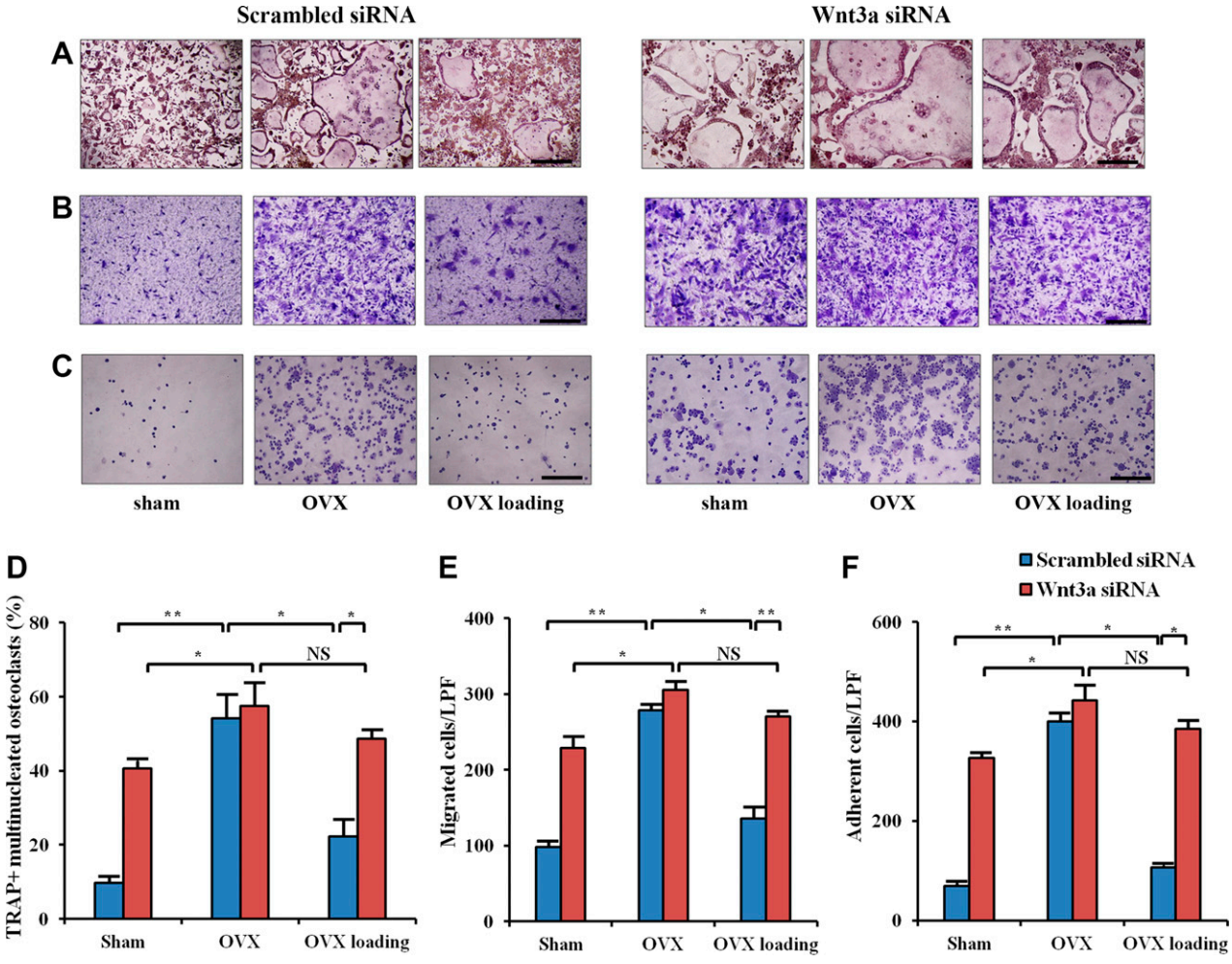

Figure 3. Effect of silencing Wnt3a on osteoclast formation, migration, and adhesion with spinal loading in OVX mice *in vitro*. *A*) Representative images of osteoclast formation by TRAP staining. *B*) Representative images of preosteoclasts migration by crystal violet staining. *C*) Representative images of preosteoclasts adhesion by crystal violet staining. *D–F*) Quantitative analysis of formation (*D*), migration (*E*), and adhesion (*F*) cells. LFP, low power field; NS, not significant. $n = 6$ per treatment group. $^*P < 0.05$, $^{**}P < 0.01$, $^{***}P < 0.001$. Scale bars, 200 μm.

β-glycerophosphate, 50 μg/ml ascorbic acid 2-phosphate, and 10 nM dexamethasone (34). Cells were fixed in citrate-buffered acetone and incubated in the alkaline-dye mix for ALP staining after being cultured for 2 wk. Cells were counterstained with Mayer's hematoxylin, and the percentages of ALP-positive cells were counted (41).

Using Alizarin Red staining to test mineralization of osteoblasts, bone marrow-derived cells were incubated for 3 wk after osteogenic differentiation. Cells were fixed in 4% paraformaldehyde for 15 min and stained with Alizarin Red S for 30 min (2% of Alizarin Red S dissolved in distilled water with the pH adjusted to 4.2). To quantify the mineral material in the culture, the stain was dissolved with 10% cetylpyridinium chloride, and the absorbance was measured at 570 nm (42).

Migration and tube formation assays of bone marrow–derived EPCs

EPCs were isolated from bone marrow–derived cells using density gradient centrifugation and cultured in 6-well dishes with selective EGM-2 (43). Prior to migration and tube formation assays, immunostaining with antibodies specific to CD34 and vascular endothelial growth factor receptor 2 (VEGFR2) was conducted to confirm that the cultured cells were EPCs (unpublished results) (44). Migration of EPCs was evaluated with 8 μm Transwell filters as previously described (45). Cells were incubated on the upper chambers, and the bottom chamber contained EGM-2 with 20% FBS. The cells in the lower chamber were stained with crystal violet and counted after 12 h. The 24-well plates were coated with Matrigel and preincubated at 37°C for tube formation assay. EPCs were incubated on the 24-well plates for 12 h, and cumulative tube lengths were counted (45).

Measurements of BMD and BMC *in vivo*

BMD and BMC were determined by peripheral dual-energy X-ray absorptiometry (pDEXA; PIXImus II; Lunar, Madison, WI, USA) (23). The animal was anesthetized and placed in the prone position, and an image was acquired in ~5 min. Both BMD (grams per square centimeter) and BMC (milligrams) of the whole body were determined without including the head. BMD and BMC of whole body, lumbar spine, humerus, ulna, femur, and tibia were also evaluated separately using mouse-specific software (Lunar, Madison, WI, USA; v.1.47).

Blood perfusion assay

We performed an ink perfusion assay using Chinese ink to analyze angiogenesis of the distal femora (34, 46). A needle with heparin-saline solution (25,000 U in 250 ml of 0.9% sodium chloride) was inserted into the left ventricle for liquid infusion. A 5% gelatin and ink solution was injected after clear liquid flowed

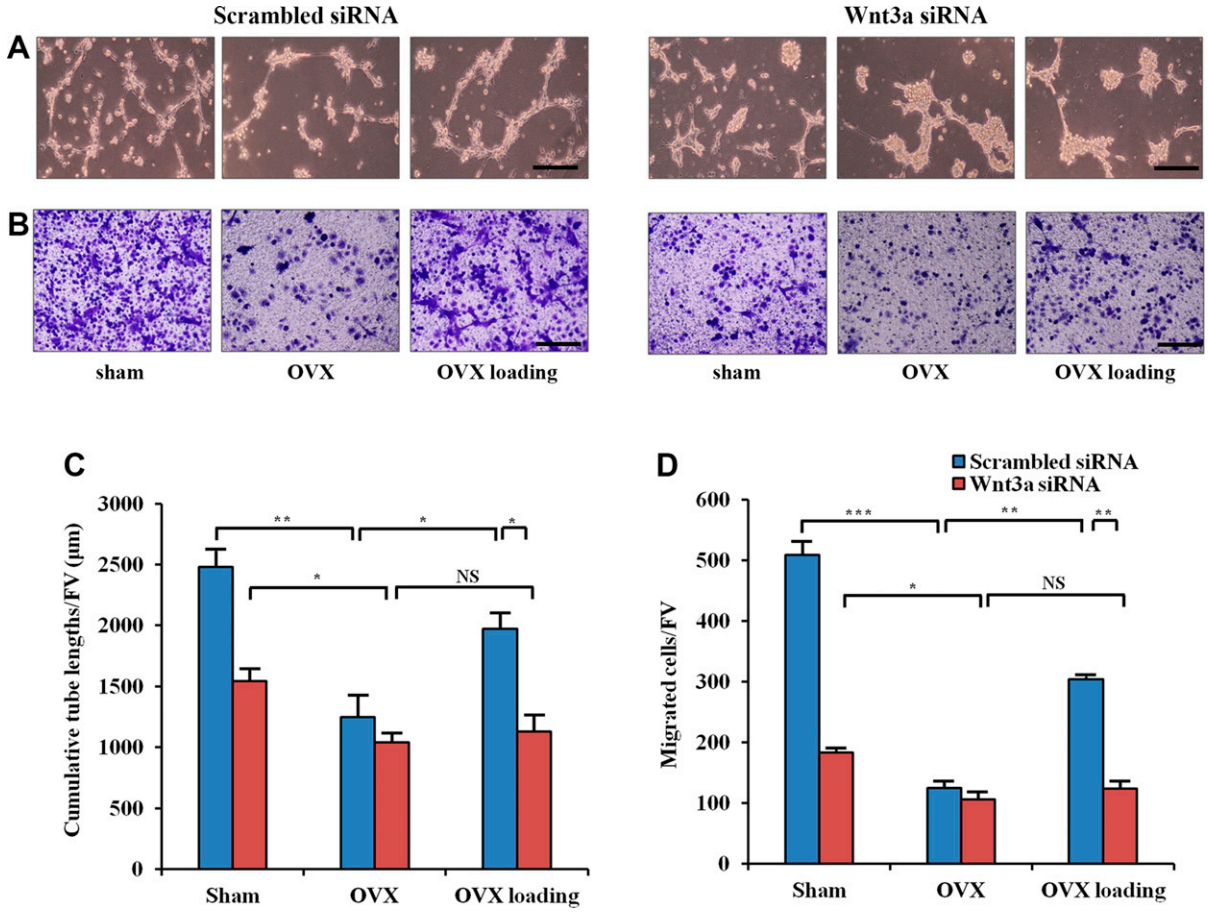

Figure 4. Effect of silencing Wnt3a on EPCs migration and tube formation with spinal loading in OVX mice *in vitro*. *A*) Representative images of EPCs tube formation. *B*) Representative images of EPCs migration by crystal violet staining. *C*) Quantitative analysis of cumulative tube lengths. *D*) Quantitative analysis of EPCs migratory. FV, field of vision; NS, not significant. $n = 6$ per treatment group. Scale bars, 100 μm. $^*P < 0.05$, $^{**}P < 0.01$, $^{***}P < 0.001$.

from the right atrium. The femora were harvested after the skin of animals became uniformly black. These tissues were fixed with 10% neutral buffered formalin for 2 d and were decalcified in 14% EDTA for 2 wk. Samples were embedded in paraffin and sectioned into 15-μm–thick slices along the sagittal plane. The ratio of a vessel area to a total area was determined.

Statistical analysis

The data were expressed as means ± SEM. For more than a 2-group comparison, 1-way ANOVA was conducted followed by a posthoc test using Fisher's protected least significant difference. For a 2-group comparison, Student's *t* test was conducted. All comparisons were 2-tailed, and statistical significance was assumed at $P < 0.05$.

RESULTS

The animals used for OVX and spinal loading tolerated the procedures, and any abnormal behavior or diminished food intake was not observed. No obvious bruising or tissue damage was detected at the surgical and loading site.

Wnt3a-mediated promotion of bone remodeling and angiogenesis by spinal loading

To evaluate the role of Wnt3a in spinal loading on OVX at the molecular level, we examined activities of Wnt3a in the femur. Immunohistochemistry and Western blot analysis showed that compared with the OVX group, the expression of Wnt3a was significantly increased by spinal loading, which also increased the protein level of β-catenin (Fig. 1*B, C*).

To further examine Wnt3a's role in bone remodeling and angiogenesis, the expressions of ALP, NFATc1, and VEGF were determined in bone marrow–derived cells in the presence and absence of siRNA specific to Wnt3a. The result showed that the levels of ALP and VEGF were increased by spinal loading, and a silencing of Wnt3a decreased load-driven up-regulation of ALP and VEGF. The level of NFATc1 was down-regulated by spinal loading, whereas transfection of Wnt3a siRNA altered the loading effect on NFATc1 (Fig. 1*D*).

Stimulation of osteoblast differentiation and mineralization by spinal loading *via* Wnt3a *in vitro*

In the osteoblast differentiation assay, a significant increase in the number of ALP-positive cells was detected in the loaded OVX mice compared with those isolated from the OVX mice ($P < 0.001$). Compared with the transfection of scrambled siRNA, Wnt3a siRNA transfection down-regulated differentiation of osteoblasts in the OVX-loading group ($P < 0.01$; **Fig. 2*A–C***).

Alizarin Red staining showed that OVX decreased the number of mineralized nodules, whereas spinal loading significantly elevated mineralization of osteoblasts ($P < 0.05$). Furthermore, a silencing of Wnt3a decreased a load-driven increase in osteoblast mineralization ($P < 0.01$; Fig. 2*B–D*).

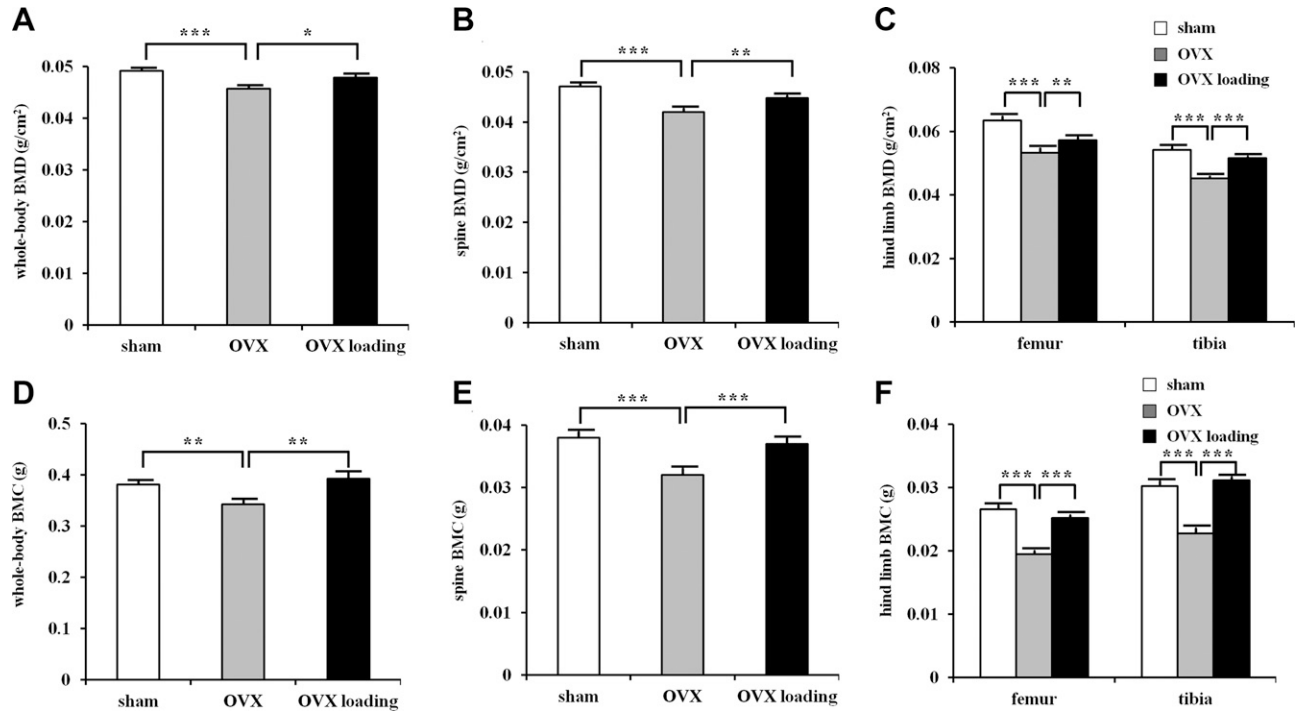

Figure 5. Effects of ovariectomy and spinal loading on BMD and BMC. *A*) BMD of whole body. *B*) BMC of whole body. *C*) BMD of lumbar spine. *D*) BMC of lumbar spine. *E*) BMD of femur and tibia. *F*) BMC of femur and tibia. $n = 10$ per treatment group; $n = 10$ for lumbar spine; $n = 20$ for femur and tibia. $^*P < 0.05$, $^{**}P < 0.01$, $^{***}P < 0.001$.

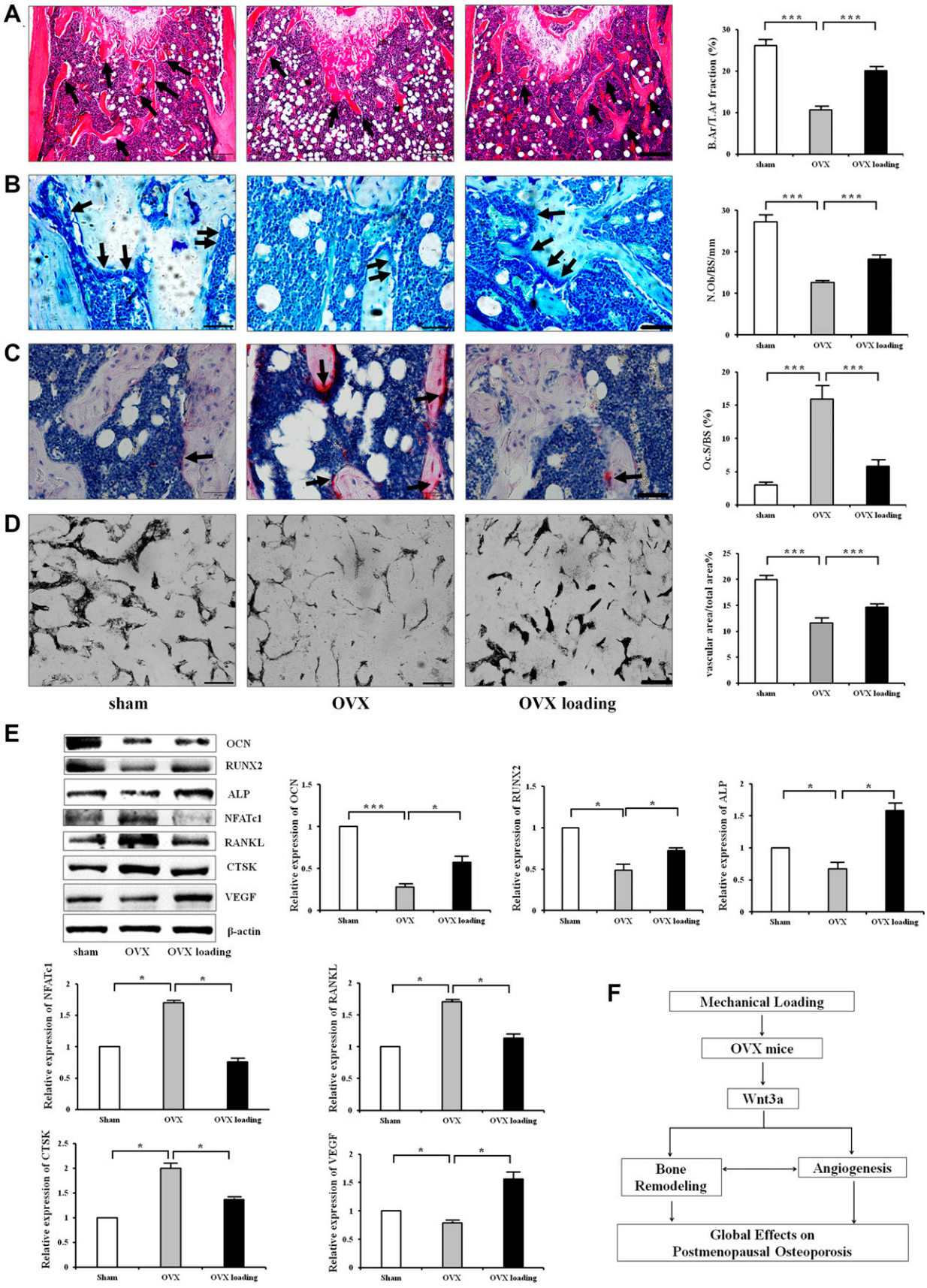

Figure 6. Effects of ovariectomy and spinal loading on bone remodeling and angiogenesis *in vivo*. *A*) The histologic parameters of trabecular bone on the proximal side of the growth plate in distal femur were determined by H&E staining. Scale bar, 200 μm; $n = 10$. The arrows indicate trabecular bone. *B*) MacNeal's staining was used to determine the number of osteoblasts in trabecular

(*continued on next page*)

Suppression of osteoclast formation, migration, and adhesion by spinal loading *via* Wnt3a *in vitro*

Four weeks after ovariectomy, the bone marrow–derived cells isolated from the OVX mice exhibited a significant increase in the surface area occupied by multinucleated osteoclasts ($P < 0.01$). In contrast, the cells isolated from the loaded OVX mice presented a significant reduction ($P < 0.05$), and transfection of Wnt3a siRNA altered load-driven reduction in osteoclast formation ($P < 0.05$; **Fig. 3*A–D***).

Preosteoclast cells isolated from the OVX mice were more active in migration than those from the sham-treated OVX mice ($P < 0.01$). In addition, preosteoclast cells isolated from the loaded mice presented a significant reduction in the migration rate ($P < 0.05$). In M-CSF–mediated adhesion to αvβ3 integrin, the cells isolated from the OVX mice presented stronger adhesion than those from the sham-treated OVX controls ($P < 0.01$). Compared with the cells isolated from the OVX mice, the cells from the spine-loaded mice exhibited a significant reduction in osteoclast adhesion ($P < 0.05$), whereas Wnt3a siRNA transfection down-regulated load-driven effects on migration ($P < 0.01$) and adhesion of osteoclasts ($P < 0.05$; Fig. 3*B–F*).

Promotion of endothelial cell migration and tube formation by spinal loading *via* Wnt3a *in vitro*

Analysis of tube formation in bone marrow–derived EPCs showed that compared with the OVX mice, spinal loading significantly increased cumulative tube lengths ($P < 0.05$) and migration of EPCs ($P < 0.01$). However, a silencing of Wnt3a decreased load-driven up-regulation of EPC migration ($P < 0.05$) and tube formation ($P < 0.01$; **Fig. 4**).

Increase in BMD and BMC by spinal loading *in vivo*

Compared with the sham-treated OVX mice 4 wk after ovariectomy, OVX mice presented a significant reduction in BMD in the whole body, lumbar spine, femur, and tibia (all $P < 0.001$). Likewise, the OVX mice showed a significant decrease in BMC in a whole body ($P < 0.01$), lumbar spine, and hind limb (both $P < 0.001$). Two-week application of daily spinal loading completely suppressed OVX-induced reduction in BMD and BMC. Compared with the OVX mice, loaded OVX mice exhibited a significant increase in BMD in whole body ($P < 0.05$), lumbar spine ($P < 0.01$), femur ($P < 0.01$), and tibia ($P < 0.001$). Similarly, spinal loading significantly elevated BMC of whole body ($P < 0.01$), lumbar spine, and hind limb (all $P < 0.001$; **Fig. 5**).

Enhancement of bone volume fraction, B.Ar/T.Ar, by spinal loading *in vivo*

Compared with the sham-treated OVX-operated mice, H&E-stained sections of the OVX mice exhibited a lower ratio of the trabecular volume to the tissue volume (B.Ar/T.Ar) in the distal femur ($P < 0.001$). Compared with the OVX group, spinal loading significantly increased B.Ar/T.Ar in the loaded OVX mice ($P < 0.001$; **Fig. 6*A***).

Inhibition of bone-resorbing osteoclasts and improvement of bone-forming osteoblasts by spinal loading *in vivo*

Compared with the sham-treated OVX group, MacNeal's staining for the OVX mice presented a significant reduction in the number of osteoblasts on the trabecular bone surface (N.Ob/BS/mm) ($P < 0.001$). However, spinal loading increased the osteoblast number in the loaded OVX mice ($P < 0.001$; Fig. 6*B*). Furthermore, the expression of osteblastic genes such as OCN, RUNX2, and ALP was significantly increased by spinal loading.

Compared with the sham-treated OVX-operated mice, TRAP staining in the distal femur showed that Oc.S/BS was significantly increased in the OVX group ($P < 0.001$). However, this increase as well as osteoclastic gene expression was significantly suppressed by spinal loading ($P < 0.001$; Fig. 6*C*). Western blot analysis showed that spinal loading also significantly decreased the protein levels of NFATc1, RANKL, and CTSK in the femur (Fig. 6).

Increase of microvascular volume by spinal loading *in vivo*

Microvessels in the distal femora of postmenopausal osteoporosis were determined using ink perfusion angiography. The OVX group had a decreased vessel area, whereas spinal loading increased it (both $P < 0.001$; Fig. 6*D*). The expression of VEGF, which is one of the most important factors in angiogenesis, was also significantly increased by spinal loading (Fig. 6*E*).

DISCUSSION

The current study demonstrates that spinal loading is able to protect from OVX-induced bone loss by

bone surface in distal metaphysis of femur. Scale bar, 50 μm; $n = 10$. Osteoblasts, located on trabecular bone surface, are indicated by the arrows. Loading-induced increase in osteoblasts numbers in OVX mice. *C*) TRAP staining was used to evaluate bone resorption in the distal metaphysis of femur. Scale bar, 50 μm; $n = 10$. TRAP-positive cells, in red, are indicated by the arrows. *D*) Ink blood perfusion angiography was used to analyze the density of microvessels. Scale bar, 100 μm; $n = 10$. *E*) Western blot showed the protein level of OCN, RUNX2, ALP, NFATc1, RANKL, CTSK, and VEGF in OVX treated with spinal loading ($n = 6$). *F*) Proposed mechanism of Wnt3a in the effect of mechanical loading on postmenopausal osteoporosis. $^*P < 0.05$, $^{**}P < 0.01$, $^{***}P < 0.001$.

promotion of bone remodeling as well as angiogenesis in a mouse model of postmenopausal osteoporosis, and Wnt3a-mediated signaling is involved in the effect of spinal loading on osteoporosis (Fig. 6*F*). The protein level of Wnt3a was increased by spinal loading, and Wnt3a siRNA altered the load-driven effects on osteoblasts and osteoclasts as well as EPCs. To further evaluate loading effects, BMD and BMC were determined. A 2-wk application of daily spinal loading significantly suppressed OVX-induced reduction in BMD and BMC. Consistent with the observed effects on BMD and BMC, the loaded OVX mice exhibited a significant increase in bone mass (B.Ar/T.Ar). Furthermore, spinal loading increased the number of osteoblasts on the trabecular bone surface, stimulating expression of OCN, RUNX2, and ALP. Spinal loading also suppressed bone resorption of osteoclasts (such as Oc.S/BS) as well as the level of the osteoclastic genes such as NFATc1, RANKL, and CTSK. Moreover, it increased microvascular volume, together with expression of VEGF. Collectively, the results indicated Wnt3a-mediated beneficial effects of spinal loading in postmenopausal osteoporosis.

A Wnt/β-catenin signaling pathway is essential for the responses to mechanical loading in bone (47). Our previous work showed that mechanical loading increased the expression Wnt3a in articular cartilage of the tibia, and it exerted protective effects on osteoarthritis by suppressing osteoclastogenesis (25). Spinal loading significantly increases the level of Wnt3a in femur after OVX. Wnt signals not only play important roles in osteoblastogenesis and osteoclastogenesis (48, 49) but also in angiogenesis (31). Though the role of Wnt3a in osteoclastogenesis was previously evaluated in *in vitro* analysis (50), the current *in vitro* and *in vivo* study is an extended analysis of the role of Wnt3a, not only in osteoclasts but also in osteoblasts and EPCs. We found that a silencing of Wnt3a decreased load-driven differentiation and mineralization of osteoblasts as well as migration and tube formation of EPCs in the OVX mice. Wnt3a siRNA increased the effects of spinal loading on formation, migration, and adhesion of osteoclasts. The load-driven effect on ALP, NFATc1, and VEGF was also altered by Wnt3a siRNA. These results indicated that Wnt3a signaling is involved in the regulation of osteoblasts, osteoclasts, and endothelial cells in response to spinal loading.

Bone remodeling is modulated by cytokines and chemokines, hormones, and biomechanical external stimuli (51). Here, spinal loading, as a unique form of mechanical stimulations, is shown to significantly restore bone quality, including the directly loaded lumbar spine as well as indirectly loaded upper limb (humerus and ulna) and hind limb (femur and tibia). Of note, spinal loading is not the only loading modality to prevent bone loss. Other stimulations, such as whole-body vibration, are reported to enhance bone formation and accelerate fracture healing (52, 53). Notably, local load application of spinal loading can exert global effects by a remote crosstalk. Our previous studies have shown that knee loading can stimulate bone formation and accelerate healing of injured bones (17–19). The result in this study showed that spinal loading elevated the osteoblast number on the trabecular bone surface of the femur. *In vitro* assays with bone marrow–derived cells showed that spinal loading stimulated differentiation and mineralization of osteoblasts, and it increased expression of the osteoblastic genes such as OCN, RUNX2, and ALP *in vivo*. These findings indicated that spinal loading is effective to promote local and global bone formation.

Antiresorption by inhibiting osteoclasts is one of the most important therapies to reduce bone loss (54). Osteoclasts originate from haemopoietic stem cells and differentiate from monocyte-macrophage lineage precursor cells. Activated osteoclasts are multinucleated cells for bone resorption (2). Postmenopausal osteoporosis is one of the osteoclast-related disorders with imbalance of bone remodeling from excessive resorption by osteoclasts (55). In this study, OVX mice showed significantly higher in Oc.S/BS *in vivo* and stimulated differentiation of multinucleated osteoclasts, stronger migration, and adhesion *in vitro* than sham-treated OVX mice. Spinal loading suppressed proliferation of preosteoclasts as well as their differentiation to mature multinucleated osteoclasts. Consistent with its effects on *in vitro* experiments, the loaded OVX mice exhibited a significant decrease in the osteoclast number on bone surface *in vivo*. Spinal loading significantly suppressed bone resorption in a mouse model of postmenopausal osteoporosis. No loaded effect on the development of osteoclasts was found in the sham-treated OVX mice (unpublished results).

Neovascularization takes place along the endosteal surface and remodeling sites of bone (56). Microvascular tissues are required for bone remodeling and play a role in coupling bone resorption and formation. The reduction of VEGF, which is one of the most important factors in angiogenesis, can be related to bone loss and a decrease in bone vascularity, possibly leading to osteoporosis (57). Herein, the effect of mechanical loading on angiogenesis in OVX mice was also evaluated. Spinal loading increased not only the microvascular volume but also expression of VEGF in the femur. The loaded OVX mice showed migration and tube formation of EPCs. Previous studies have shown the role of angiogenesis in the pathogenesis of osteoporosis (58). Our data supported the notion that enhanced angiogenesis by spinal loading contributes to preventing bone loss in the OVX mice.

In summary, the results herein demonstrate that spinal loading is effective in elevating global bone mass, BMD, and BMC and attenuating OVX-linked symptoms. The results with spinal loading are expected to provide a guideline of physical therapy for treatment of postmenopausal osteoporosis. By regulating osteoblasts and osteoclasts as well as EPCs in bone marrow, the observed beneficial outcome of spinal loading is a dual stimulatory role in bone remodeling and angiogenesis. Because the mechanism of loading effects is linked to Wnt3a, Wnt3a may serve as a therapeutic target for angiogenesis-coupled bone remodeling. FJ

ACKNOWLEDGMENTS

This work was supported by grants from National Natural Science Foundation of China (81601863 to X.L.; 81572100 and 81772405 to P.Z.), Natural Science Foundation of Tianjin (18JCQNJC82200 to X.L.), China Postdoctoral Science Foundation (2016M601275 to X.L.), and U.S. National Institutes of Health, National Institute of Arthritis and Musculoskeletal and Skin Diseases (AR052144 to H.Y.).

AUTHOR CONTRIBUTIONS

X. Li and P. Zhang designed research; X. Li, J. Li, S. Yang, J. Xu, and P. Zhang conducted research; X. Li, D. Liu, H. Yokota, and P. Zhang analyzed the data; X. Li and P. Zhang wrote the manuscript; X. Li and P. Zhang approved the final manuscript as submitted; and P. Zhang accepted responsibility for integrity of data analysis.

REFERENCES

1. Gao, C., Wei, D., Yang, H., Chen, T., and Yang, L. (2015) Nanotechnology for treating osteoporotic vertebral fractures. *Int. J. Nanomedicine* **10**, 5139–5157
2. Rachner, T. D., Khosla, S., and Hofbauer, L. C. (2011) Osteoporosis: now and the future. *Lancet* **377**, 1276–1287
3. Deng, L., Wang, Y., Peng, Y., Wu, Y., Ding, Y., Jiang, Y., Shen, Z., and Fu, Q. (2015) Osteoblast-derived microvesicles: a novel mechanism for communication between osteoblasts and osteoclasts. *Bone* **79**, 37–42
4. Kim, B. J., and Koh, J. M. (2019) Coupling factors involved in preserving bone balance. *Cell. Mol. Life Sci.* **76**, 1243–1253
5. Xu, B., Lovre, D., and Mauvais-Jarvis, F. (2016) Effect of selective estrogen receptor modulators on metabolic homeostasis. *Biochimie* **124**, 92–97
6. Li, L., Chen, X., Lv, S., Dong, M., Zhang, L., Tu, J., Yang, J., Zhang, L., Song, Y., Xu, L., and Zou, J. (2014) Influence of exercise on bone remodeling-related hormones and cytokines in ovariectomized rats: a model of postmenopausal osteoporosis. *PLoS One* **9**, e112845
7. Maraka, S., and Kennel, K. A. (2015) Bisphosphonates for the prevention and treatment of osteoporosis. *BMJ* **351**, h3783
8. Black, D. M., and Rosen, C. J. (2016) Clinical practice. Postmenopausal osteoporosis. *N. Engl. J. Med.* **374**, 254–262; erratum: 1797
9. Makras, P., Delaroudis, S., and Anastasilakis, A. D. (2015) Novel therapies for osteoporosis. *Metabolism* **64**, 1199–1214
10. Iñiguez-Ariza, N. M., and Clarke, B. L. (2015) Bone biology, signaling pathways, and therapeutic targets for osteoporosis. *Maturitas* **82**, 245–255
11. Xie, H., Cui, Z., Wang, L., Xia, Z., Hu, Y., Xian, L., Li, C., Xie, L., Crane, J., Wan, M., Zhen, G., Bian, Q., Yu, B., Chang, W., Qiu, T., Pickarski, M., Duong, L. T., Windle, J. J., Luo, X., Liao, E., and Cao, X. (2014) PDGF-BB secreted by preosteoclasts induces angiogenesis during coupling with osteogenesis. *Nat. Med.* **20**, 1270–1278
12. Zhu, K., Jiao, H., Li, S., Cao, H., Galson, D. L., Zhao, Z., Zhao, X., Lai, Y., Fan, J., Im, H. J., Chen, D., and Xiao, G. (2013) ATF4 promotes bone angiogenesis by increasing VEGF expression and release in the bone environment. *J. Bone Miner. Res.* **28**, 1870–1884
13. Alzahrani, M. M., Anam, E. A., Makhdom, A. M., Villemure, I., and Hamdy, R. C. (2014) The effect of altering the mechanical loading environment on the expression of bone regenerating molecules in cases of distraction osteogenesis. *Front. Endocrinol. (Lausanne)* **5**, 214
14. Delgado-Calle, J., Tu, X., Pacheco-Costa, R., McAndrews, K., Edwards, R., Pellegrini, G. G., Kuhlenschmidt, K., Olivos, N., Robling, A., Peacock, M., Plotkin, L. I., and Bellido, T. (2017) Control of bone anabolism in response to mechanical loading and PTH by distinct mechanisms downstream of the PTH receptor. *J. Bone Miner. Res.* **32**, 522–535
15. Shirazi-Fard, Y., Alwood, J. S., Schreurs, A. S., Castillo, A. B., and Globus, R. K. (2015) Mechanical loading causes site-specific anabolic effects on bone following exposure to ionizing radiation. *Bone* **81**, 260–269
16. Zhou, Y., Guan, X., Liu, T., Wang, X., Yu, M., Yang, G., and Wang, H. (2015) Whole body vibration improves osseointegration by up-regulating osteoblastic activity but down-regulating osteoblast-mediated osteoclastogenesis via ERK1/2 pathway. *Bone* **71**, 17–24
17. Zhang, P., Hamamura, K., Yokota, H., and Malacinski, G. M. (2009) Potential applications of pulsating joint loading in sports medicine. *Exerc. Sport Sci. Rev.* **37**, 52–56
18. Zhang, P., and Yokota, H. (2012) Elbow loading promotes longitudinal bone growth of the ulna and the humerus. *J. Bone Miner. Metab.* **30**, 31–39
19. Zhang, P., Tanaka, S. M., Jiang, H., Su, M., and Yokota, H. (2006) Diaphyseal bone formation in murine tibiae in response to knee loading. *J. Appl. Physiol.* **100**, 1452–1459
20. Zhang, P., Sun, Q., Turner, C. H., and Yokota, H. (2007) Knee loading accelerates bone healing in mice. *J. Bone Miner. Res.* **22**, 1979–1987
21. Zhang, P., Su, M., Tanaka, S. M., and Yokota, H. (2006) Knee loading stimulates cortical bone formation in murine femurs. *BMC Musculoskelet. Disord.* **7**, 73
22. Zhang, P., Turner, C. H., and Yokota, H. (2009) Joint loading-driven bone formation and signaling pathways predicted from genome-wide expression profiles. *Bone* **44**, 989–998
23. Zhang, P., and Yokota, H. (2011) Knee loading stimulates healing of mouse bone wounds in a femur neck. *Bone* **49**, 867–872
24. Liu, D., Li, X., Li, J., Yang, J., Yokota, H., and Zhang, P. (2015) Knee loading protects against osteonecrosis of the femoral head by enhancing vessel remodeling and bone healing. *Bone* **81**, 620–631
25. Li, X., Yang, J., Liu, D., Li, J., Niu, K., Feng, S., Yokota, H., and Zhang, P. (2016) Knee loading inhibits osteoclast lineage in a mouse model of osteoarthritis. *Sci. Rep.* **6**, 24668
26. Lara-Castillo, N., Kim-Weroha, N. A., Kamel, M. A., Javaheri, B., Ellies, D. L., Krumlauf, R. E., Thiagarajan, G., and Johnson, M. L. (2015) In vivo mechanical loading rapidly activates β-catenin signaling in osteocytes through a prostaglandin mediated mechanism. *Bone* **76**, 58–66
27. Holguin, N., Brodt, M. D., and Silva, M. J. (2016) Activation of Wnt signaling by mechanical loading is impaired in the bone of old mice. *J. Bone Miner. Res.* **31**, 2215–2226
28. Baron, R., and Kneissel, M. (2013) WNT signaling in bone homeostasis and disease: from human mutations to treatments. *Nat. Med.* **19**, 179–192
29. Esen, E., Chen, J., Karner, C. M., Okunade, A. L., Patterson, B. W., and Long, F. (2013) WNT-LRP5 signaling induces Warburg effect through mTORC2 activation during osteoblast differentiation. *Cell Metab.* **17**, 745–755
30. Weivoda, M. M., Ruan, M., Hachfeld, C. M., Pederson, L., Howe, A., Davey, R. A., Zajac, J. D., Kobayashi, Y., Williams, B. O., Westendorf, J. J., Khosla, S., and Oursler, M. J. (2016) Wnt signaling inhibits osteoclast differentiation by activating canonical and noncanonical cAMP/PKA pathways. *J. Bone Miner. Res.* **31**, 65–75
31. Jiang, L., Yin, M., Wei, X., Liu, J., Wang, X., Niu, C., Kang, X., Xu, J., Zhou, Z., Sun, S., Wang, X., Zheng, X., Duan, S., Yao, K., Qian, R., Sun, N., Chen, A., Wang, R., Zhang, J., Chen, S., and Meng, D. (2015) Bach1 represses Wnt/β-Catenin signaling and angiogenesis. *Circ. Res.* **117**, 364–375
32. Shuai, B., Shen, L., Yang, Y., Ma, C., Zhu, R., and Xu, X. (2015) Assessment of the impact of zoledronic acid on ovariectomized osteoporosis model using micro-CT scanning. *PLoS One* **10**, e0132104
33. Wang, W., and Fromm, M. (2015) Sphingolipids are required for efficient triacylglycerol loss in conjugated linoleic Acid treated adipocytes. *PLoS One* **10**, e0119005
34. Mussazhanova, Z., Akazawa, Y., Matsuda, K., Shichijo, K., Miura, S., Otsubo, R., Oikawa, M., Yoshiura, K., Mitsutake, N., Rogounovitch, T., Saenko, V., Kozykenova, Z., Zhetpisbaev, B., Shabdarbaeva, D., Sayakenov, N., Amantayev, B., Kondo, H., Ito, M., and Nakashima, M. (2016) Association between p53-binding protein 1 expression and genomic instability in oncocytic follicular adenoma of the thyroid. *Endocr. J.* **63**, 457–467
35. Liu, D., Zhang, Y., Li, X., Li, J., Yang, S., Xing, X., Fan, G., Yokota, H., and Zhang, P. (2017) eIF2α signaling regulates ischemic osteonecrosis through endoplasmic reticulum stress. *Sci. Rep.* **7**, 5062
36. Cheng, Z., Garikipati, V. N., Nickoloff, E., Wang, C., Polhemus, D. J., Zhou, J., Benedict, C., Khan, M., Verma, S. K., Rabinowitz, J. E., Lefer, D., and Kishore, R. (2016) Restoration of hydrogen sulfide production in diabetic mice improves reparative function of bone marrow cells. *Circulation* **134**, 1467–1483

37. Yokota, H., Hamamura, K., Chen, A., Dodge, T. R., Tanjung, N., Abedinpoor, A., and Zhang, P. (2013) Effects of salubrinal on development of osteoclasts and osteoblasts from bone marrow-derived cells. *BMC Musculoskelet. Disord.* **14**, 197
38. He, Y., Childress, P., Hood, M., Jr., Alvarez, M., Kacena, M. A., Hanlon, M., McKee, B., Bidwell, J. P., and Yang, F. C. (2013) Nmp4/CIZ suppresses the parathyroid hormone anabolic window by restricting mesenchymal stem cell and osteoprogenitor frequency. *Stem Cells Dev.* **22**, 492–500
39. Mun, S. H., Won, H. Y., Hernandez, P., Aguila, H. L., and Lee, S. K. (2013) Deletion of CD74, a putative MIF receptor, in mice enhances osteoclastogenesis and decreases bone mass. *J. Bone Miner. Res.* **28**, 948–959
40. Xiao, G., Cheng, H., Cao, H., Chen, K., Tu, Y., Yu, S., Jiao, H., Yang, S., Im, H. J., Chen, D., Chen, J., and Wu, C. (2012) Critical role of filamin-binding LIM protein 1 (FBLP-1)/migfilin in regulation of bone remodeling. *J. Biol. Chem.* **287**, 21450–21460
41. Rhodes, S. D., Wu, X., He, Y., Chen, S., Yang, H., Staser, K. W., Wang, J., Zhang, P., Jiang, C., Yokota, H., Dong, R., Peng, X., Yang, X., Murthy, S., Azhar, M., Mohammad, K. S., Xu, M., Guise, T. A., and Yang, F. C. (2013) Hyperactive transforming growth factor-β1 signaling potentiates skeletal defects in a neurofibromatosis type 1 mouse model. *J. Bone Miner. Res.* **28**, 2476–2489
42. Zhu, Y., Wang, Y., Jia, Y., Xu, J., and Chai, Y. (2019) Catalpol promotes the osteogenic differentiation of bone marrow mesenchymal stem cells via the Wnt/β-catenin pathway. *Stem Cell Res. Ther.* **10**, 37
43. Wu, J., Liu, S., Wang, Z., Ma, S., Meng, H., and Hu, J. (2018) Calcitonin gene-related peptide promotes proliferation and inhibits apoptosis in endothelial progenitor cells via inhibiting MAPK signaling. *Proteome Sci.* **16**, 18
44. Zhao, W. N., Xu, S. Q., Liang, J. F., Peng, L., Liu, H. L., Wang, Z., Fang, Q., Wang, M., Yin, W. Q., Zhang, W. J., and Lou, J. N. (2016) Endothelial progenitor cells from human fetal aorta cure diabetic foot in a rat model. *Metabolism* **65**, 1755–1767
45. Wang, S., Miao, J., Qu, M., Yang, G. Y., and Shen, L. (2017) Adiponectin modulates the function of endothelial progenitor cells via AMPK/eNOS signaling pathway. *Biochem. Biophys. Res. Commun.* **493**, 64–70
46. Fan, L., Li, J., Yu, Z., Dang, X., and Wang, K. (2014) Hypoxia-inducible factor prolyl hydroxylase inhibitor prevents steroid-associated osteonecrosis of the femoral head in rabbits by promoting angiogenesis and inhibiting apoptosis. *PLoS One* **9**, e107774
47. Javaheri, B., Stern, A. R., Lara, N., Dallas, M., Zhao, H., Liu, Y., Bonewald, L. F., and Johnson, M. L. (2014) Deletion of a single β-catenin allele in osteocytes abolishes the bone anabolic response to loading. *J. Bone Miner. Res.* **29**, 705–715
48. Karner, C. M., and Long, F. (2017) Wnt signaling and cellular metabolism in osteoblasts. *Cell. Mol. Life Sci.* **74**, 1649–1657
49. Kobayashi, Y., Uehara, S., Udagawa, N., and Takahashi, N. (2016) Regulation of bone metabolism by Wnt signals. *J. Biochem.* **159**, 387–392
50. Hamamura, K., Chen, A., Nishimura, A., Tanjung, N., Sudo, A., and Yokota, H. (2014) Predicting and validating the pathway of Wnt3a-driven suppression of osteoclastogenesis. *Cell. Signal.* **26**, 2358–2369
51. Zhang, Y., Guan, H., Li, J., Fang, Z., Chen, W., and Li, F. (2015) Amlexanox suppresses osteoclastogenesis and prevents ovariectomy-induced bone loss. *Sci. Rep.* **5**, 13575
52. Hatori, K., Camargos, G. V., Chatterjee, M., Faot, F., Sasaki, K., Duyck, J., and Vandamme, K. (2015) Single and combined effect of high-frequency loading and bisphosphonate treatment on the bone micro-architecture of ovariectomized rats. *Osteoporos. Int.* **26**, 303–313
53. Wei, F. Y., Chow, S. K., Leung, K. S., Qin, J., Guo, A., Yu, O. L., Li, G., and Cheung, W. H. (2016) Low-magnitude high-frequency vibration enhanced mesenchymal stem cell recruitment in osteoporotic fracture healing through the SDF-1/CXCR4 pathway. *Eur. Cell. Mater.* **31**, 341–354
54. Reid, I. R. (2015) Short-term and long-term effects of osteoporosis therapies. *Nat. Rev. Endocrinol.* **11**, 418–428
55. Teitelbaum, S. L., and Ross, F. P. (2003) Genetic regulation of osteoclast development and function. *Nat. Rev. Genet.* **4**, 638–649
56. Chim, S. M., Tickner, J., Chow, S. T., Kuek, V., Guo, B., Zhang, G., Rosen, V., Erber, W., and Xu, J. (2013) Angiogenic factors in bone local environment. *Cytokine Growth Factor Rev.* **24**, 297–310
57. Hu, K., and Olsen, B. R. (2016) Osteoblast-derived VEGF regulates osteoblast differentiation and bone formation during bone repair. *J. Clin. Invest.* **126**, 509–526
58. Peng, J., Lai, Z. G., Fang, Z. L., Xing, S., Hui, K., Hao, C., Jin, Q., Qi, Z., Shen, W. J., Dong, Q. N., Bing, Z. H., and Fu, D. L. (2014) Dimethyloxalylglycine prevents bone loss in ovariectomized C57BL/6J mice through enhanced angiogenesis and osteogenesis. *PLoS One* **9**, e112744; erratum: 10, e0124702

Received for publication December 22, 2018.
Accepted for publication April 8, 2019.